Article

JOURNAL OF
biomaterials
applications

Journal of Biomaterials Applications
2014, Vol 28(6) 897–908

DOI: 10.1177/0885328213486364
jba.sagepub.com
SAGE

Simvastatin-activated implant surface promotes osteoblast differentiation in vitro

Martin Sebastian Walter[1,2], Matthias Johannes Frank[1,2], Marina Rubert[3], Marta Monjo[3], Staale Petter Lyngstadaas[1] and Håvard Jostein Haugen[1]

Abstract

The bone growth promoting effects of statins suggest that these bioactive molecules can be used to improve the integration of bone-anchored implants. This study aimed at the application of simvastatin with dental implants for use in patients with low bone density. Coin-shaped titanium zirconium samples with grit-blasted and acid-etched surface were coated with simvastatin, using a novel anodic oxidation setup under alkaline conditions. The presence of intact simvastatin attached to the surface was confirmed by infrared spectroscopy. A binding site on the aliphatic O-H group was discovered and the integration of ^{1}H, ^{18}O and ^{12}C in the depth of the surface were observed by secondary ion mass spectroscopy. A simvastatin concentration of about 60 g/cm^2 was found in a release study over 72 h. The simvastatin-coated surfaces promoted alkaline phosphatase, collagen type I and osteocalcin gene expression of MC3T3-E1 cells. This suggested that the demonstrated coating holds potential for use in patients with compromised bone.

Keywords

Anodic oxidation, bioactivation, statins, titanium zirconium, implant surface analysis, osteoblast differentiation

Introduction

Statins play a major role in the modern medical world and have beneficial effects on a variety of medical conditions. While statins are commonly used as cholesterol-lowering drug, other applications involve the inhibition of tumor growth and use as anti-inflammatory drug.[1–3] In addition to this broad spectrum of applications, the use of statins for bone growth promotion has been reported.[1,4–6] Furthermore, several studies have pointed out the capability of statins to reduce bone resorption by inhibition of osteoclast activity, which makes them suitable for treatment of osteoporosis.[3,4,7–9]

The impact of statins on bone formation is mainly mediated by their stimulation of bone morphogenetic protein-2 (BMP-2), an important growth factor for osteoblast differentiation. The upregulation of BMP-2 due to the influence of statins has been proven in various studies.[1,4,5,10–12] Additionally, statins have been shown to have an inhibiting effect on HMG-CoA reductase, which subsequently leads to reduced osteoclast function.[7,8,13]

Simvastatin (SVS) belongs to the group of lipophilic statins that can enter the cell membrane by passive diffusion.[2,14,15] It is mainly used for the treatment of dyslipidemia and the prevention of cardiovascular diseases.

For the application of statins in bone healing, oral administration of the drug has been investigated.[4,16,17] Nevertheless, an increasing number of studies point out methods for local administration of statins via carrier systems. Frequently employed systems are gel or emulsion carriers[18,19] like collagen grafts.[5,6] These pathways of administration provide higher bioavailability of the drug and can be especially useful for healing of bone defects and improved osseointegration of implants.[6] The application via carriers can be done subcutaneously[1,4,17,20] or locally at bone defects.[6,11,21–23]

[1]Department of Biomaterials, Institute for Clinical Dentistry, University of Oslo, Blindern, Oslo
[2]Institute of Medical and Polymer Engineering, Chair of Medical Engineering, Technische Universität München, Garching, Germany
[3]Department of Fundamental Biology and Health Sciences, Research Institute on Health Sciences, University of Balearic Islands, Palma de Mallorca, Spain

Corresponding author:
Håvard Jostein Haugen, Faculty for Dentistry, PO box 1109, Oslo, NO-0317, Norway.
Email: h.j.haugen@odont.uio.no

Nevertheless, there is only one study that demonstrates the application of SVS directly on a surface by oxygen plasma modification.[24] Therefore, the attachment of SVS by anodic oxidation directly to an implant system could be a possible option for local administration of SVS.

This study aimed at SVS immobilization on a commercially available implant surface by application of anodic oxidation in a weak alkaline NaOH solution. The surface was comparable to the Roxolid® SLActive® surface by Institut Straumann AG (Basel, Switzerland). Attachment and integrity of SVS on the surface were analyzed with Fourier transformed infrared spectroscopy (FTIR), X-ray photoelectron spectroscopy (XPS), secondary ion mass spectroscopy (SIMS) and UV visible spectroscopy (UV-VIS). For assessment of topographical and morphological surface changes, field emission SEM (FE-SEM), blue-light profilometer, and optical microscope were used. An in vitro study using MC3T3-E1 cells was performed to evaluate the biological effects of this novel implant surface activation.

Material and methods

Sample preparation

The samples used in this study were coin shaped with a diameter of 6.25 mm and a height of 2 mm. Smaller coins with a diameter of 4.39 mm and 2 mm of height were used for the in vitro study. All coins were made from a titanium zirconium alloy (TiZr) with a zirconium content of 13%–17%. The samples were grit blasted and acid etched in hydrochloric and sulfuric acid (SBAE). After production, handling and packaging was done under nitrogen cover gas and the samples were stored in 0.9% NaCl, making the surfaces comparable to the commercially available SLActive® surface (Institut Straumann AG, Basel, Switzerland).[25,26]

The test coins were unpacked under laminar flow and washed for 5 min in an ultrasound bath with deionized water prior to the electrocoating process. An electolyte with 200 mL deionized water, adjusted to a pH of 8.5 with 600 µL of 0.01 M NaOH was used. An SVS stock solution with a concentration of 20 mg/mL was prepared in 100% ethanol. To achieve a final concentration of 0.1 µg/mL, 1 mL of SVS stock solution was added in the electrolyte.

Platinum cathode, Ti electrode and stirrer were cleaned with 100% pure ethanol and rinsed in sterile water prior to the anodic oxidation. The TiZr coins were mounted on individual titanium holders, teflon caps protected the interface between the holder and the coin from the electrolyte. The coins were kept wet at all times until process start. The custom-made coating setup put out a current of 0.88 mA/cm^2 for every coin at a treatment time of 75 min. Coins for the in vitro study were prepared in the same fashion but were treated for 1 h at a current density of 5.03 mA/cm^2. After the process, the SVS-coated coins were dried in nitrogen gas flow and packed in containers filled with nitrogen prior to further analysis. TiZr SBAE coins were used as control and were washed, dried and packed according to the same protocol. The only exception from the cover gas packaging were the coins analyzed in SIMS.

Coating homogeneity

A Leica DMRB Fluorescence Microscope (Wetzlar, Germany) was used for the optical assessment of the coin surface. Main focus was homogeneity and color shade differences in comparison to untreated TiZr SBAE coins. The microscope was used with external lighting. A ×1.25 objective was used, which in combination with the camera system added up to a total of ×12.5 magnification.

Chemical surface composition and binding

The diffuse reflectance (DR) accessory of a PerkinElmer Spectrum 400 FTIR/FTNIR spectrometer (PerkinElmer, Waltham, MA, USA) was used to analyze SVS-coated and TiZr SBAE coins in order to compensate for the rough surfaces. After recording of a background spectrum from an untreated TiZr SBAE coin, the samples were scanned on three different spots each. Furthermore, attenuated total reflectance (ATR) was used to measure pure SVS powder. The scans were executed on a wavelength between 500 cm^{-1} and 4000 cm^{-1} in the mid infrared region. Every measurement was constituted of 8 individual measurements with a resolution of 8 cm^{-1}. The scans were normalized and manually baseline corrected after the measurements. Furthermore, transformation to absorbance was done for the scan of pure SVS.

The XPS analysis was carried out on an Axis Ultra^{DLD} XP spectrometer (Kratos Analytical, Manchester, UK) using monochromatic Al Kα radiation ($h\nu = 1486.6$ eV). Survey spectra were recorded in a range between 1100 eV and 0 eV binding energy (BE). Detail spectra were acquired in the energy regions of O1 s, Ti2p and C1 s. The instrument resolution was 1.1 eV for the survey scans and 0.55 eV for the detail scans. The analysis area was 300 µm × 700 µm. Samples were mounted on a sample bar with conductive carbon tape. The energy shift due to surface charging was below 1 eV based on the C1 s peak position relative to established BEs, therefore the experiment was performed without charge compensation. All BEs

were energy referenced based on the C1 s peak at 284.5 eV BE.

Depth integration of SVS

The oxygen, carbon and hydride profiles on the test coins were measured by SIMS (Cameca IMS 7f, Paris, France). The analysis was carried out for ^{1}H, ^{18}O, ^{12}C ions on 8 SVS-coated and 1 TiZr SBAE sample. A 50-nA primary beam of 15 keV Cs^{+} was used for rastering over a surface area of 200 µm × 200 µm, while negative secondary ions were collected from central part (67 µm × 67 µm) of the crater at room temperature. The depth of each sputtering crater was analyzed by a blue light profilometer (Sensofar Pll 2300, Terrassa, Spain), and the aspect heights were calculated using an advanced software package (Sensomap, Sensofar, Terrassa, Spain). The crater depth was measured with a × 50 objective (50 × PI, Nikon, Tokyo, Japan) over an extended topography of 2 × 2 images, each with a viewing area of 253 µm × 190 µm at 20% overlapping. Because of the rough surface topography, a special fine-shift algorithm was used for surface scanning. The result data from the SIMS measurement was calibrated according to the obtained crater depth.

Total SVS concentration and release

The release experiment was carried out with 0.5 mL of a 60% acetonitrile and 3% trifluoroacetic-acid mixture (ACN-TFA), which was added to the samples in microcentrifuge tubes (Axygen Microtubes, United City, CA, USA). Samples were stored on a shaker at room temperature at a frequency of 300 r/min to provide permanent sample movement. At timepoints of 4 h, 16 h, 48 h and 72 h, 3.5 µL of release fluid were extracted and measured with UV-VIS.

For the analysis of SVS content in the release fluid, a Nano-drop ND 1000 spectrometer (Thermo Fisher Scientific, Waltham, MA, USA) in UV-VIS mode was used. A standard curve for SVS was recorded for concentrations between 0.005 mg/mL and 0.25 mg/mL of SVS in ACN-TFA. The absorption was measured for all samples and the standard curve at 238 nm.

Surface structure

An analytical assessment of the surface topography and morphology was done with a blue light laser profilometer (A PLµ2300, Sensofar-Tech S.L., Terrassa, Spain) using a 50 × EPI (Nikon, Tokyo, Japan) confocal objective. The datasets were analyzed with the topography software Sensomap 4.1 Plus (Sensofar-Tech S.L., Terrassa, Spain). The following surface amplitude parameters were analyzed to compare the materials: Total surface area in percent of a completely flat surface (S_{dr}), average roughness (S_a), total height of the surface (S_t), skewness of the height distribution (S_{sk}), kurtosis of the height distribution (S_{ku}) and core fluid retention index (S_{ci}).

All FE-SEM-images were obtained with a Quanta 200 FEG (FEI Hillsboro, Oregon, USA) microscope. Samples were sputtered with platinum prior to imaging. The samples were measured on a 45° tilted stage with a working distance between 6 mm and 7.5 mm. High vacuum mode was used for all samples to record images with 20.000× and 50.000× resolution.

Bioactivity and bioavailability

The mouse osteoblastic cell line MC3T3-E1 was obtained from the German Collection of Microorganisms and Cell Cultures (DSMZ, Braunschweig, Germany). MC3T3-E1 cells were routinely cultured at 37°C in a humidified atmosphere of 5% CO_2 and maintained in α-MEM supplemented with 10% fetal calf serum (FCS) and antibiotics (50 IU penicillin/mL and 50 µg streptomycin/ml). Cells were subcultured 1:50 before reaching confluency using PBS and trypsin/EDTA. All experiments were performed in the same passage of the MC3T3-E1 cells (passage 16). The coins were placed in a 96-well plate (4.5 mm well) and 7×10^3 cells were seeded on each well to study cell differentiation and cell toxicity. The same number of cells were cultured in parallel in TCP dishes in all experiments. Trypan blue stain was used to determine total and viable cell number. For the experiments, MC3T3-E1 cells were maintained for 14 days on the implants in α-MEM supplemented with 10% FCS and antibiotics. Culture media was changed every other day. Culture media was collected after 24 h to test the toxicity of the treatments and of the different implant surfaces (LDH activity). To study cell diffentiation, cells were harvested at 14 days and Coll-1, ALP and OC gene expression were analysed using real-time RT-PCR.

The presence of LDH activity in the culture media after 24 h was used as an index of cell death. LDH activity was determined spectrophotometrically after 30 min incubation, following the procedures of the manufacturer (Roche Diagnostics, Mannheim, Germany). Results were presented relative to the LDH activity present in the cell culture media collected from cells seeded on plastic culture (TCP) dishes and incubated with Triton X-100 at 1% (Positive control, 100% cytotoxicity) and from cell culture media from cells seeded on TCP dishes without any treatment (Negative control, 0% cytotoxicity).

Total RNA was isolated with Tripure (Roche Diagnostics, Mannheim, Germany), following the

instructions of the manufacturer. RNA was quantified using a spectrophotometer set at 260 nm (ND 1000 spectrometer, Thermo Fisher Scientific, Waltham, MA, USA).

Real-time RT-PCR was performed for 2 housekeeping genes, 18 S ribosomal RNA (18S rRNA), glyceraldehyde-3-phosphate dehydrogenase (GAPDH) and 3 target genes, ALP, Col-I and OC. Primers sequences used have been reported earlier.[12]

The same amount of total RNA (0.25 μg) from each sample was reverse transcribed to cDNA at 37°C for 60 min in a final volume of 20 mL, using high-capacity RNA to cDNA kit (Applied Biosystems, Foster City, CA, USA). Each cDNA was diluted 1/4. A negative control without cDNA template was run in each assay. Real-time PCR was performed using the Light Cycler FastStar DNA Master PLUS SYBR Green I (Roche Diagnostics, Mannheim, Germany) following the manufacture's instructions. The concentration of PCR reaction components, amplification program and quantification were done as documented earlier.[27]

Real-time efficiencies were calculated from the given slopes in the LightCycler 480 software using serial dilutions, showing all the investigated transcripts high real-time PCR efficiency rates, and high linearity when different concentrations are used. PCR products were subjected to a melting curve analysis on the LightCycler and subsequently 2% agarose/TAE gel electrophoresis to confirm amplification specificity, the primer melting temperature and amplicon size, respectively.

Relative quantification after PCR was calculated by dividing the concentration of the target gene in each sample by the mean of the concentration of the two reference genes (housekeeping genes) in the same sample using the advanced relative quantification method provided by the LightCycler 480 analysis software version 1.5 (Roche Diagnostics, Mannheim, Germany).

Statistics and data analysis

All data gained from the SIMS analysis were scaled to the actual crater depth from the profilometer analysis by converting sputtering time to depth. Thus, all time values were multiplied by the mean difference of measured crater depth and maximum sputtering time using Excel 2007 (Microsoft, Redmond, WA, USA). The depth at which the hydride concentration reaches its maximum was determined by using the MAX-function in Excel 2007. The total amount of an isotope was determined by calculating the area beneath the graph by calculating the integral of the curve using Origin 8 (OriginLab, Guangzhou, China). The advanced graphing and analysis software SigmaPlot 11 (Systat Software, San José, CA, USA) was used for data plotting. Statistical analysis was executed with SigmaStat 11 (Systat Software, San José, CA, USA). The analysis of the profilometer results was done with ANOVA on ranks. For further statistical analysis of the in vitro results paired *t*-test was used. Differences were considered significant (*) for $p \leq 0.05$ and highly significant (**) for $p \leq 0.01$, and labeled, respectively.

Results

Coating homogeneity

Pictures of the surfaces recorded with an optical microscope are displayed in Figure 1. Coins coated with SVS adopted a distinct purple color after the coating, while TiZr SBAE control coins had a bright grey color. The color shade was homogenous over the coin surface.

Chemical surface composition and binding

FTIR analysis of the SVS-coated coins and pure SVS powder is displayed in Figure 2. Peaks of the pure SVS powder were more distinct than on the SVS-coated samples. Absorbance values were furthermore found to be lower on the SVS-coated samples. The peak at 1714 cm^{-1} was identified in as carbonyl C = O stretch, as well as the more distinct peaks on the SVS powder at 1723 cm^{-1} and 1695 cm^{-1}. The former represented an ester and the latter an aromatic carbonyl group.[28–30] The peak at 1461 cm^{-1} appeared on pure SVS powder at 1467 cm^{-1} and was derived from C-H methylene bending.[30,31] The spectrum of SVS-coated coins showed another peak at 1387 cm^{-1}, while two peaks at 1389 cm^{-1} and 1369 cm^{-1} were observed on pure SVS powder, both of which were due to C-H bending.[30,29] The peak at 1256 cm^{-1} on the coated samples was derived from a C-O-C lactone stretch and was resolved in two peaks at 2166 cm^{-1} and 1225 cm^{-1} on pure SVS powder.[30] The peak at 1162 cm^{-1} on pure SVS and 1159 cm^{-1} on SVS-coated samples was due to a C-O-C ester stretch. Also, a peak at 1053 cm^{-1} on SVS-coated samples appeared in two individual peaks at 1072 cm^{-1} and 1055 cm^{-1} for pure SVS powder. Both of these peaks were from C-O stretching of secondary alcohol according to Elbary et al.[30] Small peak shifts to lower wavelengths were observed on SVS-coated samples, yet, the occurrence of these shifts could be explained by the combination of two adjoining peaks in the SVS-coated samples. Nevertheless, in the high-frequency region above 3000 cm^{-1}, a peak corresponding to free alcohol O-H stretching at 3548 cm^{-1} on the pure SVS powder was shifted to 3448 cm^{-1} on the SVS-coated sample.[30]

The XPS analysis was performed to evaluate the chemical bonding of SVS on the surface. Figure 3

Figure 1. Surface analysis of simvastatin coating.

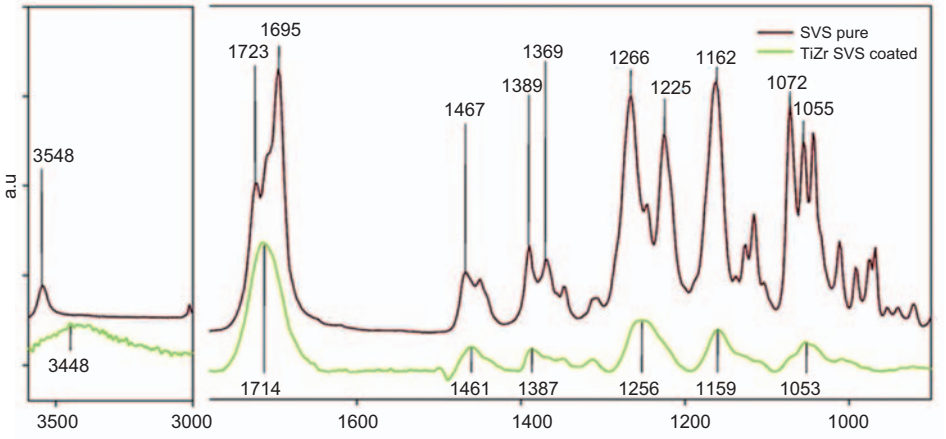

Figure 2. FTIR curves of SVS coating. SVS pure (upper graph) and TiZr SVS coated (lower graph). Characteristic absorbance peaks are marked.

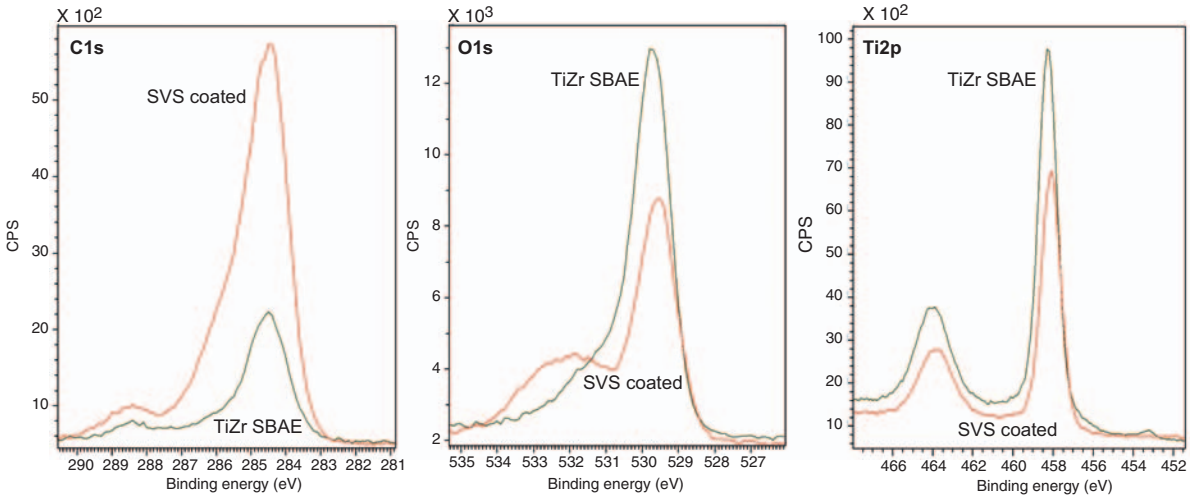

Figure 3. XPS detail spectra of C1s, O1s and Ti2p. SVS coated and TiZr SBAE.

shows the detail spectra of C1s, O1s and Ti2p. It could be observed that the intensity of the carbon peaks increased, whereas the peaks for titanium were reduced on the SVS-coated sample in comparison to the control TiZr SBAE. The C1s peak was referenced to 284.5 eV according to Moulder et al.[32] This peak, corresponding to C-H and C-C bonds, was strongly increased on the SVS-coated sample. In addition, the carbon signal of the SVS-coated sample exhibited a shoulder at 285.5 eV from C-O, which was nearly not visible on the TiZr SBAE sample. The peak at 288.5 eV corresponding to O-C = O was visible on both samples in similar intensity. The Ti2p 3/2 peak was found at 458 eV and the Ti2p 1/2 peak 5.5 eV higher. Oxygen from O^{2-} was found at 529.5 eV on both samples but was lowered on the SVS-coated sample. In contrast, the contribution from OH^{-} at 523.3 eV was strongly increased on the SVS-coated sample.

Depth integration of SVS

SIMS measurements were obtained from ^{1}H, ^{12}C and ^{18}O isotopes in order to investigate the depth integration of those elements. SVS inclusion in the surface was detected by analysis of the depth profile of the ^{12}C isotope (Figure 4). The ^{1}H isotope showed higher peak intensity for the SVS-coated samples in comparison to the TiZr SBAE samples. The depth of the hydrogen layer was approximately 1.5 µm for both samples. While hydrogen was not present in the outer layer of the SVS-coated sample, TiZr SBAE showed a very high initial intensity with the maximum at a depth of 0.034 µm. In contrast, high hydrogen concentrations could be observed on the SVS-coated sample, reaching a maximum at 0.065 µm. The maximum count intensity was 1.27E + 07 c/s for SVS-coated and 7.15E + 06 c/s for TiZr SBAE, which was a 77% increase for SVS-coated in comparison to TiZr SBAE (Table 1). The total area of hydrogen was increased 46% on SVS-coated samples, which corresponded to the total amount of hydrogen.

The ^{12}C isotope was found increased on SVS-coated samples with a maximum of 5.85E + 04 c/s at depth of 0.02 µm, whereas the TiZr SBAE sample had the maximum concentration directly at the surface and decreased continuously (Figure 4). The ^{12}C layer depth, which should correspond to the inclusion of SVS in the surface, was visible up to 0.5 µm in SVS-coated samples. For TiZr SBAE, the depth was lower and not as well defined. The total amount of ^{12}C was 19% higher on the SVS-coated samples, yet it was more depth integrated than on the TiZr SBAE samples (Table 1).

Oxygen ^{18}O was considerably higher on SVS-coated samples from the outermost point of the surface. While increasing intensity was found for ^{18}O in SVS-coated samples with a maximum of 2.15E + 5 c/s at a depth of 0.021 µm, oxygen levels decreased continuously for TiZr SBAE (Figure 4).

Total SVS concentration and release

Figure 5 displays the amount of SVS released from eight SVS-coated coins over a period of 72 h. Release was performed in ACN-TFA, as prior attempts with water and simulated body fluid (SBF) were not successful. After 72 h no more SVS was released from the coins and the experiment was stopped. Within the first 4 h an average of 42.5 µg/cm^2 were released from the coins, which was the highest release within two time points. Between 4 h and 16 h, the average amount of SVS released was 13.15 µg/cm^2. After 48 h, an additional 2.20 µg/cm^2 were released.

Surface structure

The surface characterization with profilometer showed significantly increased total surface area on the SVS-coated samples in comparison to untreated TiZr SBAE. Furthermore, significant decrease was found for the parameter S_{ku}, which displays the surface kurtosis.[33] All other parameters analyzed did not show any

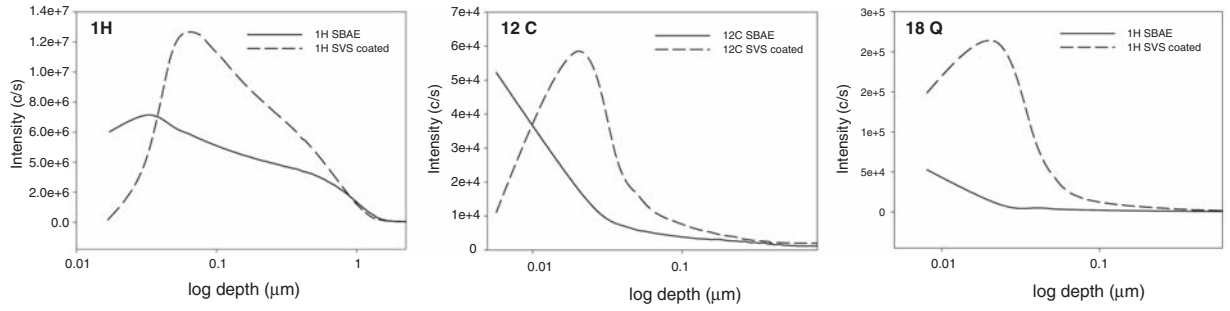

Figure 4. Depth profiles of ^{1}H, ^{12}C and ^{18}O of simvastatin (SVS)-coated coins and one control.

significant changes due to the process. The total height of the surface (S_t) was decreased to 96% of TiZr SBAE on doxy-coated coins, arithmetic mean summit curvature of the surface (S_{ci}), roughness average (S_a) and skewness of the height distribution (S_{sk}) showed even less changes (Table 2).

A high-resolution FE-SEM analysis is displayed in Figure 6. Surface topography and morphology showed differences between the groups, yet, the morphological changes from the coating were more distinct than the topographical changes. The lower resolution images showed a rough surface for TiZr SBAE with the concave indents of grit blasting still visible. Edges were sharp and the peaks very distinct. In contrast to that, the SVS-coated sample showed few relics of grit blasting. The surface consisted of numerous independent rounded peaks. It seemed much smoother, yet had numerous very fine and deep valleys in between the peaks. Several bright spherical structures were visible all over the surface with a diameter between 50 nm and 150 nm.

The higher magnification images showed the rougher TiZr SBAE surface in detail. Different areas on the surface were separated clearly and the surface displayed some spherical white structures in the range between 50 nm and 100 nm. In contrast, the SVS-coated surface was very smooth and showed surface coverage in a homogenous way. White spherical structures were visible all over the surface with a diameter of 50 nm to 150 nm.

In vitro bioactivity and bioavailability

We next investigated the effect of SVS-coated TiZr implants on MC3T3-E1 cell viability after 24 h and compared to control surfaces (TiZr SBAE) under the same conditions. As seen in Figure 7, a significant increase was found for the SVS-coated samples compared to TiZr SBAE, although this increase was only of about 17% compared to the reference TCP surface. In contrast, TiZr SBAE surfaces showed lower cytotoxicity than TCP.

Furthermore, the gene expression of several markers related to proliferative stage of osteoblasts (Col-I), matrix maturation and differentiation (ALP), mineralization (OC) was analyzed to investigate the effect of SVS-coated TiZr implants on the differentiation of MC3T3-E1 osteoblasts after 14 days of cell culture (Figure 7). Although all these markers were increased in SVS-coated samples, only Col-I and OC showed significant differences compared to TiZr SBAE surfaces.

Discussion

The precipitation of molecules by NaOH and heat treatment of titanium has been described in the literature earlier.[34] Yet, these methods were commonly used to attach relatively small molecules like CaP. Successful attachment of more complex molecules like statins has not been reported to the best of our knowledge. The mechanism used in NaOH treatment, as well as for

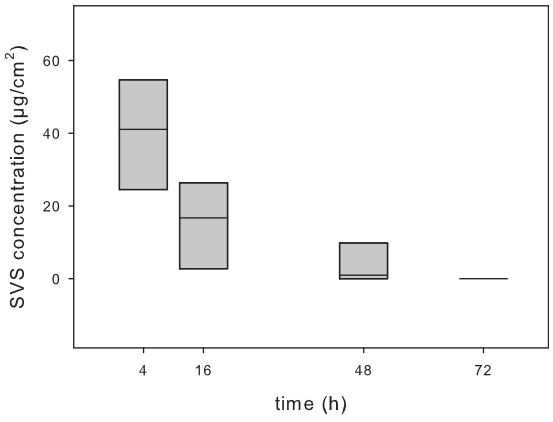

Figure 5. Simvastatin (SVS) release over 72 h. Measurements taken at 4 h, 16 h, 48 h and 72 h. Amount calculated in µg/cm^2. Graph displays the amounts released between the time points.

Table 1. SIMS maximum concentration of hydrogen and carbon depth profiles in c/s*μm. Total content was calculated with an algorithm for integration over curves in Origin. The mathematical area was calculated with the lowest and highest depth values as limits.

Sample	^{1}H maximum intensity (c/s)	^{12}C maximum intensity (c/s)	^{1}H total content (c/s * µm)	^{12}C total content (c/s * µm)
SVS-coated (average)	1.27E + 07	5.85E + 04	5.36E + 06	8.21E + 03
TiZr SBAE	7.15E + 06	5.23E + 04	3.65E + 06	6.86E + 03
Difference (%)	77.62	11.85	46.85	19.68

attachment by plasma treatment, is based on the build-up of OH-groups on the sample surface.[34,35] OH^- built by anodic oxidation showed also promising results for binding of CaP.[36–38] Due to the constant current applied and the continuous production of OH-groups, anodic oxidation is also suitable for attachment of more complex molecules. In theory, the attachment of molecules like SVS could be established during anodic oxidation by the release of Ti^{4+} ions. These ions possess low solubility at pH 8 and therefore bind to liberated OH^- and O^{2-}, but also to the SVS in solution. Therefore, it was expected that SVS would be present on the surface after the coating, as well as an increased amount of OH-groups.

Proof of binding

No major peak shift between pure SVS powder and the SVS-coated samples was observed for the region below 2000 cm^{-1} in FTIR, which indicated that the molecule was intact on the surface. The peaks on the pure SVS powder were more resolved, as peaks on the SVS-coated samples were usually present in two or more peaks in the spectrum of the powder. This effect could be attributed to lower measurement efficiency on the rough SVS-coated samples in comparison to the pure SVS powder.[39] The peak corresponding to free alcohol O-H stretching on pure SVS powder, which was found at 3548 cm^{-1} in accordance with the literature, was shifted to 3448 cm^{-1} on the SVS-coated sample.[30] As the peak was shifted and its intensity was strongly decreased, it was assumed, that the O-H component of SVS binds to the surface with Ti^{4+} and is therefore immobilized. Due to a proton transfer at the OH group of SVS, it could be bound to the surface via anodic oxidation in alkaline pH.[40,41]

The bonding of SVS was assessed with XPS to analyze changes in functional groups on the surface due to the coating process. The decrease in the Ti2p signal intensity was a strong indicator for masking of the original surface.[42] Furthermore, an increase in carbon from C-H / C-C as well as C-O indicated the presence of the molecule on the surface, as the samples were always stored in nitrogen cover gas to minimize the influence of environmental carbon contamination. An increase in OH-groups was observed on the surface after the coating, which supported the assumption

Table 2. Average surface analysis parameters. ANOVA on ranks showed significant differences for S_{dr} ($p = 0.011$) and S_{ku} ($p = 0.017$), marked with *.

	S_{dr} (%)	S_{ci}	S_t (μm)	S_a (μm)	S_{sk}	S_{ku}
TiZr SBAE	67.82	1.37	21.03	1.55	−0.41	4.74
SVS-coated	88.49*	1.40	20.28	1.59	−0.42	3.57*

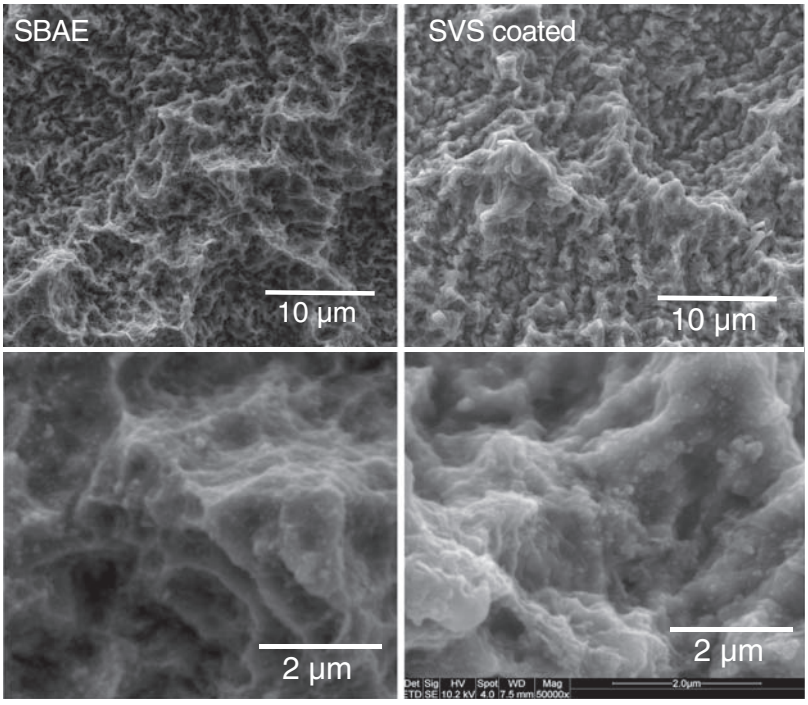

Figure 6. SEM analysis of titanium zirconium alloy (TiZr) SBAE and simvastatin (SVS)-coated samples; 10 μm scalebar displays ×20.000 magnification, 2 μm scalebar represents ×50.000.

that SVS was integrated into the surface by binding of its OH component (Figure 3). The activation of a surface by production of OH-groups on the surface has been reported in the literature earlier.[35,43] Nevertheless, it is unlikely in this context that the OH-groups observed on the surface in the XPS analysis were solely derived from the SVS bound on the surface, a certain percentage was surely from attachment of OH^- from the electrolyte solution. Due to this uncertainty regarding the dominance of the SVS binding process, the amount of SVS had to be analyzed in a release experiment.

Investigations by SIMS measurements aimed at the further assessment of the binding and the depth integration of the molecule into the surface. It could be seen that all displayed profiles of ^{1}H, ^{12}C and ^{18}O had the point of maximum intensity shifted towards deeper layers on the SVS-coated samples (Figure 4). Therefore, an integration of SVS into the depth of the sample surface was likely. The increased ^{1}H and ^{18}O concentration and total content were probably due to a buildup of OH-groups, as well as an integration and binding of the OH-groups from SVS.[44] In contrast, the higher ^{12}C amount and concentration was most likely owed to the carbon in SVS, even though samples were not protected from environmental carbon. It was visible that the untreated TiZr SBAE sample picked up carbon in a different way than the SVS-coated sample (Figure 4). While the untreated TiZr SBAE sample had the highest concentration on the outer sample surface, with concentration rapidly decreasing with depth, the SVS-coated samples had a more integrated carbon depth profile, which was attributed to SVS. In contrast, the carbon on the TiZr SBAE sample was probably due to environmental carbon contamination.[45]

Biomolecule content and release kinetics

Further support for a strong binding of SVS to the samples surface was found in the release study, which evaluated the behavior of SVS release from the sample coins (Figure 5). As attempts with water or SBF as release medium were not successful, release conditions with ACN-TFA had to be used. This mixture was chosen due to the properties of ACN and TFA as strong organic solvents.[46,47] Therefore, it was not

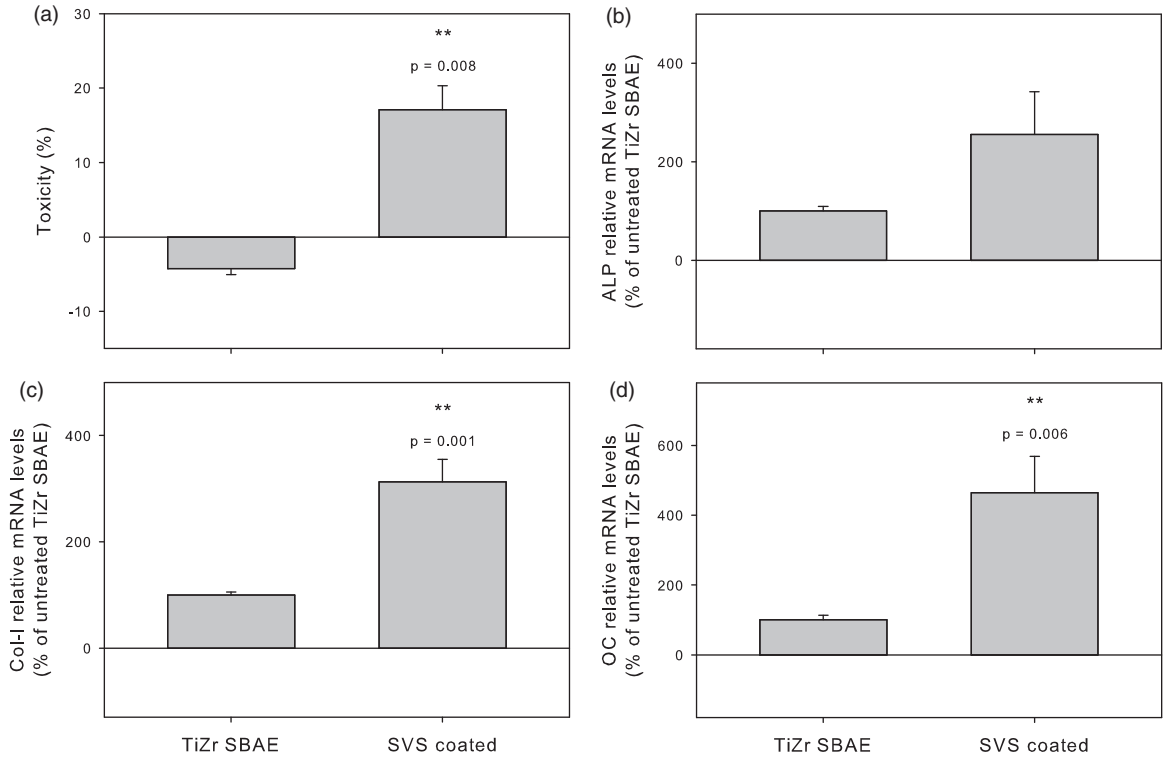

Figure 7. LDH activity ALP, Col-I and ALP OC mRNA levels on simvastatin (SVS)-coated and titanium zirconium alloy (TiZr) SBAE samples. (a) LDH activity measured from culture media of MC3T3-E1 cells seeded on coin samples. Positive control (100%) was cell culture media from cells seeded on TCP dishes and incubated with Triton X-100 at 1%. Negative control (0%) was cell culture media from cells seeded on TCP dishes without any treatment. (b) ALP mRNA levels compared to TiZr SBAE (100%). Coll-ICol-I and OC relative mRNA levels on SVS-coated and TiZr SBAE samples. (c) Coll-ICol-I mRNA activity (d) OC mRNA levels. Values referenced to TiZr SBAE (100%). Values represent the mean ±SEM. Paired t-test: *for $p \leq 0.05$; ** for $p \leq 0.01$.

surprising that the major part of the SVS on the samples was released after 4 h already. Yet, with a total release time of 72 h until complete depletion of SVS in the samples, a slow release was more probable under in vivo conditions than a burst release. The Nano-drop analysis revealed a substantial amount of SVS released from the samples, which suggested that the major part of the OH-groups detected in XPS were due to attachment of SVS.

Effects on roughness and morphology

Modification of TiZr SBAE surfaces by SVS coating increased the total surface area of the surfaces and decreased the surface kurtosis. Decreasing S_{ku} values indicated rounder shaped peaks after the coating process.[33] This was in accordance with the decrease in S_t, which showed a general flattening of the total height of surface structures. Yet, with increasing S_{dr} values, surface structures that added to the total surface area had to be formed during the process.

With regard to the FE-SEM pictures from Figure 6, the modification of the surface became clearer. The whole surface of the SVS-coated samples showed modified morphology; especially the disappearance of sharp edges and the creation of rounded structures suggested the buildup of a surface layer containing SVS. The rounded peak shapes were in concordance with the profilometer results. Furthermore, the appearance of fine deep valleys suggested the validity of release of Ti^{4+} ions in the pits that combined with SVS and reattached the surface.

In vitro bioactivity and bioavailability

One of the most important prerequisites for the use of a biomaterial is a high level of biocompatibility.[48] LDH is a stable cytoplasmatic enzyme present in all cells, which is rapidly released into the cell supernatant upon damage of the plasma membrane, and thus represents a measurement of cytotoxicity.[49] In the present work, we used the cell supernatant and a short-term incubation of MC3T3-E1 cells with the different TiZr surfaces to avoid possible differences with the number of cells. Thus, we found a 17% increase in cytotoxicity in the cell supernatant after 24 h in the SVS-coated TiZr implants, although this treatment did not impair MC3T3-E1 cell differentiation after 14 days. In fact, gene expression analysis of several differentiation markers pointed to an increased differentiation in the SVS-coated samples. Thus, despite the initial increased cytotoxicity, the results illustrated the occurrence of SVS's typical effect on the gene expression, as increased levels of ALP, Col-I and OC were described by Maeda et al.[2,4,10] Interestingly, numerous reports suggest that statins have also effects independent of their cholesterol lowering ability. For instance, SVS can promote osteoblast viability and differentiation via membrane-bound Ras/Smad/Erk/BMP-2 pathway.[50] The most plausible explanation for the increased differentiation of MC3T3-E1 cells cultured on SVS-coated implants is that this biomolecule becomes bioavailable to the cells due to the reversible covalent bonds between SVS and the metal surface. The most important statement in this context was therefore the bioavailability of SVS to the cells and the positive effect of SVS on cell differentiation.

Conclusion

The study successfully proved the binding of SVS to a TiZr SBAE surface by means of anodic oxidation. The FTIR analysis found SVS intact on the surface and a method of binding the SVS after combination of aliphatic O-H with Ti^{4+} was suggested. This method of binding was furthermore supported by the XPS analysis showing an increased amount of OH-groups on the SVS-coated samples. Integration of SVS in the sample surface was documented by the SIMS analysis, showing increased ^{1}H, ^{18}O and ^{12}C isotopes. The release of the molecule over 72 h showed an SVS concentration of nearly 60 $\mu g/cm^2$ on the surfaces. Effective release under harsh conditions was detected up to 48 h after start of the experiment, suggesting a slow release under physiological conditions. The coating of the surface was furthermore demonstrated by high resolution FE-SEM images. The SVS on the sample surfaces was available for the osteoblastic cells and positively influenced their differentiation. As a positive effect on the mRNA levels of ALP, Col-I and OC was found, the bioactivity of SVS could be demonstrated.

References

1. Garrett I, Gutierrez G and Mundy G. Statins and bone formation. *Curr Pharm Des* 2001; 7(8): 715–736.
2. Liao J and Laufs U. Pleiotropic effects of statins. *Annu Rev Pharmacol Toxicol* 2005; 45: 89–118.
3. Tandon V, Bano G, Khajuria V, et al. Pleiotropic effects of statins. *Indian J Pharmacol* 2005; 37(2): 77–785.
4. Mundy G, Garrett R, Harris S, et al. Stimulation of bone formation in vitro and in rodents by statins. *Science* 1999; 286(5446): 1946–1949.
5. Wong R and Rabie A. Histologic and ultrastructural study on statin graft in rabbit skulls. *Int J Oral Maxillofac Surg* 2005; 63(10): 1515–1521.
6. Monjo M, Rubert M, Wohlfahrt JC, et al. In vivo performance of absorbable collagen sponges with rosuvastatin in critical-size cortical bone defects. *Acta Biomater* 2009; 6(4): 1405–1412.

7. Uzzan B, Cohen R, Nicolas P, et al. Effects of statins on bone mineral density: a meta-analysis of clinical studies. *Bone* 2007; 40(6): 1581–1587.
8. Staal A, Frith J, French M, et al. The ability of statins to inhibit bone resorption is directly related to their inhibitory effect on HMG-CoA reductase activity. *J Bone Miner Res* 2003; 18: 88–96.
9. Kaji H, Kanatani M, Sugimoto T, et al. Statins modulate the levels of osteoprotegerin/receptor activator of NFkappaB ligand mRNA in mouse bone-cell cultures. *Horm Metab Res* 2005; 37(10): 589–592.
10. Maeda T, Matsunuma A, Kurahashi I, et al. Induction of osteoblast differentiation indices by statins in MC3T3-E1 cells. *J Cell Biochem* 2004; 92: 458–471.
11. Ayukawa Y, Yasukawa E, Moriyama Y, et al. Local application of statin promotes bone repair through the suppression of osteoclasts and the enhancement of osteoblasts at bone-healing sites in rats. *Oral Surg Oral Med Oral Pathol Oral Radiol Endod* 2009; 107(3): 336–342.
12. Monjo M, Rubert M, Ellingsen J, et al. Rosuvastatin promotes osteoblast differentiation and regulates SLCO1A1 transporter gene expression in MC3T3-E1 cells. *Cell Physiol Biochem* 2010; 26(4–5): 647–656.
13. Grasser W, Baumann A, Petras S, et al. Regulation of osteoclast differentiation by statins. *J Musculoskelet Neuronal Interact* 2003; 3(1): 53–62.
14. Pagkalos J, Cha JM, Kang Y, et al. Simvastatin induces osteogenic differentiation of murine embryonic stem cells. *J Bone Miner Res* 2010; 25(11): 2470–2478.
15. Hamelin B and Turgeon J. Hydrophilicity/lipophilicity: relevance for the pharmacology and clinical effects of HMG-CoA reductase inhibitors. *Trends Pharmacol Sci* 1998; 19(1): 26–37.
16. Oxlund H and Andreassen TT. Simvastatin treatment partially prevents ovariectomy-induced bone loss while increasing cortical bone formation. *Bone* 2004; 34(4): 609–618.
17. Anbinder AL, Junqueira JC, Mancini MNG, et al. Influence of simvastatin on bone regeneration of tibial defects and blood cholesterol level in rats. *Braz Dent J* 2006; 17: 267–273.
18. Kang BK, Lee JS, Chon SK, et al. Development of self-microemulsifying drug delivery systems (SMEDDS) for oral bioavailability enhancement of simvastatin in beagle dogs. *Int J Pharm* 2004; 274(1–2): 65–73.
19. Thylin MR, McConnell JC, Schmid MJ, et al. Effects of simvastatin gels on murine calvarial bone. *J Periodontol* 2002; 73(10): 1141–1148.
20. Hughes A, Rogers MJ, Idris AI, et al. A comparison between the effects of hydrophobic and hydrophilic statins on osteoclast function in vitro and ovariectomy-induced bone loss in vivo. *Calcif Tissue Int* 2007; 81(5): 403–413.
21. Ayukawa Y, Okamura A and Koyano K. Simvastatin promotes osteogenesis around titanium implants. *Clin Oral Implants Res* 2004; 15(3): 346–350.
22. Moriyama Y, Ayukawa Y, Ogino Y, et al. Topical application of statin affects bone healing around implants. *Clin Oral Implants Res* 2008; 19(6): 600–605.
23. Seto H, Ohba H, Tokunaga K, et al. Topical administration of simvastatin recovers alveolar bone loss in rats. *J Periodontal Res* 2008; 43(3): 261–267.
24. Yoshinari M, Hayakawa T, Matsuzaka K, et al. Oxygen plasma surface modification enhances immobilization of simvastatin acid. *Biomed Res* 2006; 27(1): 29–36.
25. Rupp F, Scheideler L, Olshanska N, et al. Enhancing surface free energy and hydrophilicity through chemical modification of microstructured titanium implant surfaces. *J Biomed Mater Res A* 2006; 76(2): 323–334.
26. Szmukler-Moncler S, Bischof M, Nedir R, et al. Titanium hydride and hydrogen concentration in acid-etched commercially pure titanium and titanium alloy implants: a comparative analysis of five implant systems. *Clin Oral Implants Res* 2010; 21(9): 944–950.
27. Satué M, Petzold C, Córdoba A, et al. Uv Photoactivation of 7-dehydrocholesterol on titanium implants enhances osteoblast differentiation and decreases rankl gene expression. *Acta Biomater* 2012; 9(3): 5759–5770.
28. Ryan JA, Compton SV, Brooks MA, et al. Rapid verification of identity and content of drug formulations using mid-infrared spectroscopy. *J Pharm Biomed Anal* 1991; 9(4): 303–310.
29. Bal T and Murthy P. Studies of drug-polymer interactions of simvastatin with various polymers. *Int J Pharm Sci Res* 2012; 3: 561–563.
30. Abd Elbary A, Ibrahim HK and Hazaa BS. Formulation and evaluation of colon targeted tablets containing simvastatin solid dispersion. *Drug Ther Studies* 2011; 1(1): e16.
31. Socrates G. *Infrared and Raman characteristic group frequencies: Tables and charts*. Hoboken, NJ, USA: John Wiley & Sons; 2001.
32. Moulder JF and Chastain J. *Handbook of X-ray photoelectron spectroscopy*. MN: Perkin-Elmer Eden Prairie, 1992.
33. Lamolle S, Monjo M, Lyngstadaas S, et al. Titanium implant surface modification by cathodic reduction in hydrofluoric acid: Surface characterization and in vivo performance. *J Biomed Mater Res A* 2009; 88A(3): 581–588.
34. Wen HB, Wolke JGC, de Wijn JR, et al. Fast precipitation of calcium phosphate layers on titanium induced by simple chemical treatments. *Biomaterials* 1997; 18(22): 1471–1478.
35. Yoshinari M, Matsuzaka K and Inoue T. Surface modification by cold-plasma technique for dental implants—Bio-functionalization with binding pharmaceuticals. *Jpn Dent Sci Rev* 2011; 47(2): 89–101.
36. Ishizawa H and Ogino M. Characterization of thin hydroxyapatite layers formed on anodic titanium oxide films containing Ca and P by hydrothermal treatment. *J Biomed Mater Res* 1995; 29(9): 1071–1079.
37. Ishizawa H and Ogino M. Formation and characterization of anodic titanium oxide films containing Ca and P. *J Biomed Mater Res* 1995; 29(1): 65–72.
38. Zhu X, Kim KH and Jeong Y. Anodic oxide films containing Ca and P of titanium biomaterial. *Biomaterials* 2001; 22(16): 2199–2206.

39. Schmitt J and Flemming HC. FTIR-spectroscopy in microbial and material analysis. *Int Biodeterior Biodegrad* 1998; 41(1): 1–11.
40. Sharma P, Denny WA and Garg S. Effect of wet milling process on the solid state of indomethacin and simvastatin. *Int J Pharm* 2009; 380(1–2): 40–48.
41. Ellingsen JE, Lyngstadaas SP. Medical prosthetic devices having improved biocompatibility. Patent 20080269910, USA, 2008.
42. Fleming GJ, Adib K, Rodriguez JA, et al. Proline adsorption on TiO_2(110) single crystal surface: A study by high resolution photoelectron spectroscopy. *Surf Sci* 2007; 601(24): 5726–5731.
43. Yoshinari M, Takemoto S, Hattori M, et al. (eds). Immobilization of simvastatin acid onto titanium with plasma surface modification. In: *Proceedings of the scientific meeting of Japanese Medical Society for biological interface*; 2005, vol. 41, p. 19.
44. McCafferty E, Wightman J and Cromer TF. Surface properties of hydroxyl groups in the air-formed oxide film on titanium. *J Electro Soc* 1999; 146(8): 2849–2852.
45. Lausmaa J. Surface spectroscopic characterization of titanium implant materials. *J Electron Spectros Relat Phenomena* 1996; 81(3): 343–361.
46. Mahoney WC and Hermodson MA. Separation of large denatured peptides by reverse phase high performance liquid chromatography. Trifluoroacetic acid as a peptide solvent. *J Biol Chem* 1980; 255(23): 11199–11203.
47. Walter M and Ramaley L. Purification of acetonitrile. *Anal Chem* 1973; 45(1): 165–166.
48. Van Tienhoven EAE, Korbee D, Schipper L, et al. In vitro and in vivo (cyto)toxicity assays using PVC and LDPE as model materials. *J Biomed Mater Res A* 2006; 78A(1): 175–182.
49. Decker T and Lohmann-Matthes M-L. A quick and simple method for the quantitation of lactate dehydrogenase release in measurements of cellular cytotoxicity and tumor necrosis factor (TNF) activity. *J Immunol Method* 1988; 115(1): 61–69.
50. Chen P-Y, Sun J-S, Tsuang Y-H, et al. Simvastatin promotes osteoblast viability and differentiation via Ras/Smad/Erk/BMP-2 signaling pathway. *Nutr Res* 2010; 30(3): 191–199.